Journal of Materials Chemistry A

Accepted Manuscript

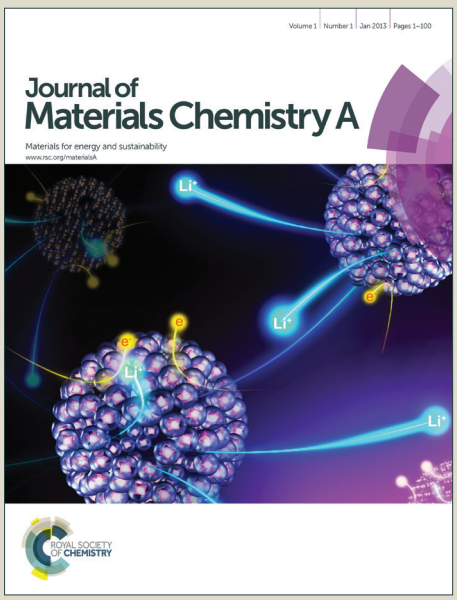

ROYAL SOCIETY OF CHEMISTRY

www.rsc.org/materialsA

RSCPublishing

COMMUNICATION

Fabrication of metal-oxide-free $CH_3NH_3PbI_3$ perovskite solar cells processed at low temperature

Cite this: DOI: 10.1039/x0xx00000x

Seongchan Ryu,[a,§] Jangwon Seo,[a,§] Seong Sik Shin,[a] Young Chan Kim,[a] Nam Joong Jeon,[a] Jun Hong Noh,[a] and Sang Il Seok*[,ab]

Received 00th January 2014,
Accepted 00th January 2014

DOI: 10.1039/x0xx00000x

www.rsc.org/

Efficient, metal-oxide-free perovskite solar cells were successfully developed by employing the N-I-P architecture. The modified solvent engineering process employing a diethylether drip as an orthogonal solvent enabled fabrication of a multi-layered device comprising FTO/PEI/PCBM/$MAPbI_3$/PTAA/Au at low temperature (≤100 ˚C). Optimization of the thickness of the phenyl-C61-butyric acid methyl ester (PCBM) layer in the planar device yielded an overall power conversion efficiency (PCE) of 15.3% with a large hysteresis but a steady-state efficiency of 13.9% under AM 1.5G 100 mW·cm^{-2} illumination. The use of the low-temperature processed dense-TiO_2 layer in conjunction with the PCBM layer gave rise to performance comparable to that of the single electron transport layer (ETL) device and enabled fabrication of an efficient, flexible perovskite solar cell with a PCE of 11.1%.

Hybrid organic/inorganic lead halide perovskite materials with the formula $CH_3NH_3PbI_3$ (= $MAPbI_3$) are characterized by good intrinsic properties for photovoltaic applications. These properties include an excellent optical band gap that can be tuned by varying the chemical composition, high absorption coefficient, long hole-electron diffusion length, and good carrier transport.[1-17] Great success has been achieved in the development of perovskite solar cells employing the N-I-P architecture comprising mesoporous (mp)-TiO_2 /perovskite material/hole-transport material (HTM).[18-19] The certified power conversion efficiency (PCE) of these systems has already exceeded 20%, a feat accomplished by the present group.[20]

Despite the high performance of mesostructured perovskite solar cells, high-temperature processing (>450 °C) is required for preparing mp-TiO_2. This requirement is an obstacle for commercial manufacture.[21-23] Therefore, other recent efforts to realize a low-temperature, easily fabricated, and flexible perovskite solar cell have focused on optimization of a simple planar heterojunction device using a compact charge collection layer without a mesoporous scaffold.[23-25] This approach is also expected to pave the way for large-scale production using conventional solution processing techniques such as slot-die coating, spray coating, and roll-to-roll processing, etc.[26,27] To this end, several electron transport layer (ETL) materials, such as TiO_2, ZnO, and TiO_2-graphene composites fabricated at low temperature (<150 ˚C), have been successfully applied to the development of prototype high performance perovskite solar cells.[22,23,25] Very recently, an efficiency of 19.3% was achieved with a device employing yttrium-doped TiO_2.[24] However, we demonstrated that large hysteresis in the *J-V* curve measured in the forward and reverse bias scans is more severe in the planar architecture than in the mesostructured perovskite solar cell.[18] Furthermore, a more pronounced decline of the average efficiency of the planar device was also found with a slower scan rate, and there was a continued decline in average value from the reverse and forward scans.[18]

In addition to metal-oxides, phenyl-C61-butyric acid methyl ester (PCBM) is also recognized as a promising candidate as an n-type material for use in solar cells, and has already been utilized in the P-I-N architecture,[28-35] i.e., the so-called normal organic photovoltaic configuration, but has been relatively under-utilized in the N-I-P architecture due to the lack of acceptable processes for deposition of a uniform and dense perovskite layer on PCBM. The performance of P-I-N solar cells employing ITO/poly(3,4-ethylenedioxythiophene):poly(styrenesulfonic acid) (PEDOT:PSS)/$MAPbI_3$/PCBM/Al is still low compared to N-I-P devices employing a compact TiO_2 and ZnO layer. Moreover, the acidic and hygroscopic nature of PEDOT:PSS and the oxygen-sensitivity of the Al metal electrode have a negative impact on the long-term stability.[36] Therefore, positioning of PCBM as a single ETL in the front of perovskite layers, i.e., the N-I-P architecture, is important for fabrication of efficient and stable perovskite solar cells.

Recently, we reported the use of a solvent-engineering process employing a mixture solution comprising dimethyl sulfoxide (DMSO):γ-butyrolactone (GBL) (3:7, v/v) to form a high-quality, flat perovskite film with full coverage, which is essential for fabrication of efficient perovskite solar cells.[18] The formation of DMSO-PbI_2 complexes aids in retardation of rapid crystallization between the inorganic PbI_2 and CH_3NH_3I components. During consecutive spin-coating processes, dripping of a non-solvent (like toluene) allows formation of a smoother film by removing the residual spin-coating solvents along with DMSO. Subsequent thermal annealing induces rapid crystallization to create a highly crystalline and uniform perovskite film.

Herein, we report the fabrication of efficient perovskite solar cells based on the FTO/PEI/PCBM/$CH_3NH_3PbI_3$/PTAA (polytriarylamine)/Au configuration by combining a PCBM ETL and modified solvent engineering process. A maximal overall PCE of 15.3% with a large hysteresis but steady-state efficiency of 13.9% under AM 1.5G 100 mW·cm^{-2} illumination are achieved with the optimized cell. The simultaneous use of a low-temperature processed dense-TiO_2 layer and the PCBM layer resulted in performance comparable to that of single PCBM, and enabled fabrication of an efficient, flexible perovskite solar cell with a PCE of 11.1%.

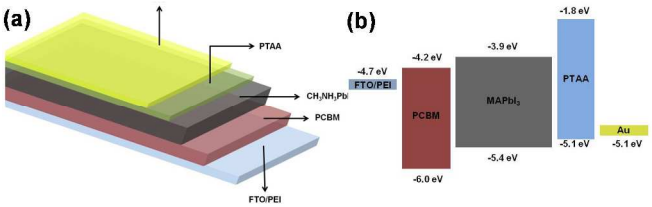

Fig. 1. (a) Device architecture of the FTO/PEI/PCBM/$CH_3NH_3PbI_3$/PTAA/Au cells and (b) energy levels of the various device layers.

Fig. 1a displays the device structure of the hybrid planar PCBM-$MAPbI_3$ heterojunction solar cell (FTO/PEI/PCBM/$CH_3NH_3PbI_3$/PTAA/Au) and the energy level diagram of each layer in the device. The FTO substrate was first coated with an extremely thin layer of polyethyleneimine (PEI) as an interfacial material. The role of PEI is well-known in inverted polymer solar cells, where it modifies the work function of the FTO (or ITO) cathode due to the strong electrostatic self-assembled dipoles, and facilitates electron extraction into the electrode via fullerene derivatives.[37,38] The orthogonal solubility of PEI enabled the deposition of the PCBM layer onto the FTO/PEI substrate. From the energy band alignment of the PCBM-$MAPbI_3$ heterojunction shown in Fig. 1b, free charge carriers (or excitons) generated in the $MAPbI_3$ layer can be extracted (or dissociated) by electron transfer to PCBM. The electrodes collect the photogenerated free carriers; the FTO/PEI assembly collects electrons via PCBM, and Au metal collects the holes through the PTAA polymer.

A metal-oxide free N-I-P perovskite solar cell based on the PCBM-$MAPbI_3$ heterojunction was successfully fabricated by judicious selection of an orthogonal solvent for establishing a $MAPbI_3$ film on top of the PCBM layer. As displayed in Fig. 2a and 2b, the amorphous PCBM layer covers the entire surface area of the FTO/PEI assembly without pin-hole defects, even though a rough morphology arises from the uneven FTO substrate. For orthogonal solvent processing, a robust solvent resistance of the bottom PCBM layer against the spin coating solvents for the upper layers is necessary. Generally, a limited number of polar solvents (*N,N*-dimethylformamide (DMF), dimethyl sulfoxide (DMSO), and γ-butyrolactone (GBL)) is employed for formation of the perovskite film. Such polar solvents are relatively marginal solvents for the PCBM layer within the short exposure time (less than a couple of minutes) during spin coating. Finally, PTAA as a HTM polymer was deposited on top of the perovskite film using non-polar toluene as a solvent in which the PCBM layer beneath the perovskite film is also soluble. It should be noted that 100% perfect surface coverage of a thick perovskite film on top of PCBM is crucial for the use of the PCBM layer in place of TiO_2. This requirement has generally limited the applicability of PCBM in the N-I-P architecture, despite the tremendous efforts to deposit a uniform and dense perovskite film with a well-controlled morphology using several solution processing methods such as one-step precursor deposition, sequential deposition, and vapour-assisted solution processes. Thus, the present solvent engineering technique is highly desirable as a faster and facile one-step precursor solution processing method for achieving a metal-oxide free N-I-P perovskite solar cell using PCBM. However, as explained earlier, this solvent engineering process utilizes the toluene drip, which induces damage in the PCBM layer. To address this limitation, several solvents in which both PCBM and $MAPbI_3$ have minimal solubility were screened with the expectation that these solvents should not be deleterious during spin coating. At the same time, such dripping solvents must satisfactorily create a uniform and flat perovskite film, similar to that obtained using toluene.

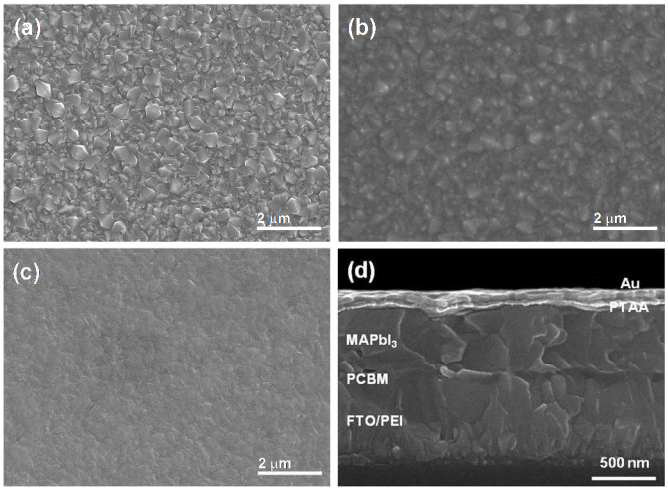

Fig. 2. SEM image of top surface of (a) FTO/PEI, (b) FTO/PEI/PCBM and (c) FTO/PEI/PCBM/$MAPbI_3$. (d) Cross-sectional SEM image showing the device structure of the PCBM-$CH_3NH_3PbI_3$ bilayer heterojunction solar cell.

To find an ideal dripping solvent for the solvent engineering process, a series of solvents (diethylether, 2-propanol, acetonitrile, and tetrahydrofuran) were evaluated, giving rise to totally different

morphologies as observed in the SEM images (see Fig. S1). Acetonitrile and tetrahydrofuran were ineffective for generating the perovskite film. Moreover, the PCBM layer was still damaged during spin coating, resulting in exposure of the FTO/PEI surface. With the use of diethylether and 2-propanol, the dripping solvent induced formation of a pale-brown colored film that further became black upon subsequent annealing at 100 °C for 30 min. As shown in Fig. 2c and Fig. S1, a uniform and flat layer with submicron-sized grains perfectly covered the entire surface. The absorption spectrum of the film obtained using diethylether dripping was typical of $CH_3NH_3PbI_3$ over the entire UV and visible range up to 800 nm (see Fig. S2). Thus, by judicious selection of an appropriate orthogonal solvent in the present modified solvent engineering process, we successfully fabricated a multi-layered device with the FTO/PEI/PCBM/$MAPbI_3$/PTAA/Au configuration. This is evidenced by the cross-section of the device shown in Fig. 2d, which clearly indicates the presence of each layer of PCBM (~80 nm), $MAPbI_3$ (450~500 nm), and PTAA (~50 nm), along with both electrodes.

The photocurrent density-voltage (*J-V*) curves of the PCBM-$MAPbI_3$ heterojunction obtained using these devices are presented in Fig. 3. The device fabricated using 2-propanol as a dripping solvent exhibited a rather low PCE (<1%), even though the device was successfully fabricated (not shown here).

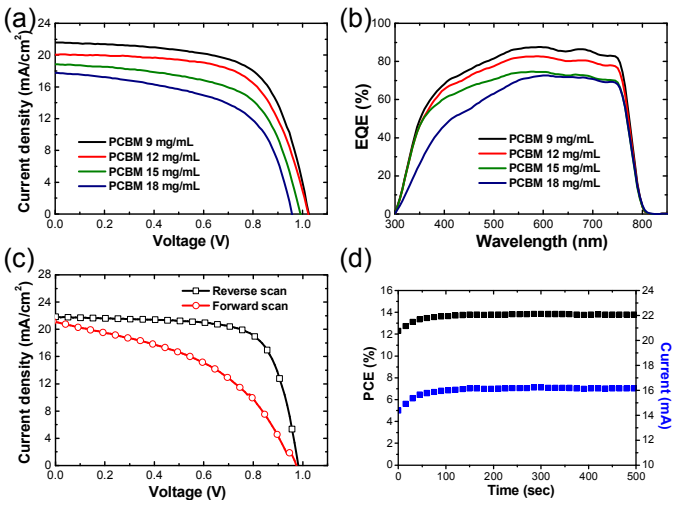

Fig 3. (a) Photocurrent density-voltage (*J-V*) characteristics of PCBM-$CH_3NH_3PbI_3$ heterojunction solar cells with respective PCBM layer thicknesses of 45 (black), 55 (red), 80 (green), and 100 nm (blue), measured under simulated AM 1.5 100 mW cm^{-2} sunlight. (b) Corresponding external quantum efficiency (EQE) spectra of PCBM-$CH_3NH_3PbI_3$ heterojunction solar cells with respective PCBM layer thicknesses of 45 (black), 55 (red), 80 (green), and 100 nm (blue). (c) *J-V* characteristics of the optimal PCBM-$CH_3NH_3PbI_3$ heterojunction solar cell device with PCBM layer thickness of 55 nm under reverse (black) and forward (red) bias scan, and (d) its steady-state efficiency (black) with the photocurrent (red) as a function of time applied at a forward bias of 0.82 V.

To optimize the PCBM layer in this device, the thickness of the PCBM layer was controlled by varying the concentration of the PCBM spin-coating solution. Film thicknesses of 45, 55, 80, and 100 nm were obtained using PCBM concentrations of 9, 12, 15, and 18 mg/mL, respectively, while keeping all other conditions the same. As shown in Fig. 3a, the PCE of the device increased from 9.8% to 14.4% with decreasing thickness of the PCBM layer. The details of the device parameters are presented in Table 1. The short circuit current density (J_{sc}), open circuit voltage (V_{oc}), and fill factor (*FF*) followed a similar trend. The V_{oc} reached almost 1.0 V. However, the variation in the V_{oc} was less than 0.07 V. In contrast, the J_{sc} was found to increase significantly from 17.8 to 21.6 mA·cm^2 as the PCBM layer became thinner, which is explained by the corresponding external quantum efficiency (EQE) spectra in Fig. 3b. For the 45-nm- and 55-nm-thick PCBM layer device, the EQE profile shows a broad peak in the range of 300 nm to 800 nm owing to the absorbance of the thick $MAPbI_3$ layer. Interestingly, no significant reduction of the EQE associated with the absorption of the PCBM film was observed; however, minimal optical loss is likely to inevitably occur based on the device configuration where the incident photon reaches the light-absorbing $MAPbI_3$ layer through the PCBM layer. It was known that PCBM has a weak absorption band at ~343 nm with a long tail in the visible range, even though the molar extinction coefficient of 4,900 mol^{-1}·cm^{-1} at 400 nm and <1,000 mol^{-1}·cm^{-1} at 650 nm is not high.[39] Thus, it is reasonable that the thicker PCBM layer affected the EQE spectra, resulting in a relatively lower contribution in the range below 500 nm relative to in the longer wavelength range. Furthermore, the decreasing trend of the EQE over the total range implies that charge collection is inefficient for the device with the thicker PCBM layer. This is probably attributed to increased recombination when the dissociated electrons are extracted toward the FTO/PEI electrode over the longer distance in the thick PCBM layer [36]. For the device with the 140 nm thick PCBM layer, in particular, the current density and the fill factor were quite low.

Table 1. Device parameters of PCBM-$CH_3NH_3PbI_3$ heterojunction solar cells depending on PCBM concentration; measured under simulated AM 1.5 100 mW cm^{-2} illumination.

PCBM (mg/mL)	J_{sc} (mA/cm^2)	V_{oc} (V)	FF	PCE (%)
9	21.6	1.02	0.65	14.4
12	20.1	1.02	0.64	13.3
15	18.9	0.989	0.62	11.5
18	17.8	0.955	0.58	9.8

Therefore, the more reliable device with the 55 nm thick PCBM layer was further optimized to achieve a PCE of 15.3% with a J_{sc} of 21.8 mA cm^{-2}, a V_{oc} of 0.98 V, and a *FF* of 72%, as shown in Fig. 3c. It is noted that the optimal efficiency achieved herein is comparable to that of perovskite solar cells fabricated with a thin film of TiO_2 or ZnO without a mesoporous layer. Recently, unexpected hysteresis in the *J-V* curve of these planar heterojunction solar cells has been reported based on the scan direction and scan rate. For accurate estimation of the PCE, measuring the steady-state maximum power output at a fixed forward bias has been suggested as a feasible method by Snaith and McGehee.[40,41] They also reported that in a planar heterojunction devices, the steady-state efficiency declined significantly relative to that measured in the reverse bias scan. As shown in Fig. 3c, hysteresis was observed in the *J-V* curves of the present cell, i.e., 15.3% and 9.8% for the reverse and forward bias scans, measured with 10 mV voltage steps and a delay time of 40 ms. This trend is similar to those observed with the planar geometry. However, a steady-state PCE of 13.9% was obtained herein by measuring the stabilized photocurrent held at a forward

bias of 0.82 V (see Fig. 3d). Only a 1.4% drop in efficiency was observed as compared to that in the reverse bias scan, unlike other cells employing only dense-TiO_2.

This study represents the first successful report of introduction of the PCBM layer into the N-I-P architecture as a single ETL for fabrication of efficient planar heterojunction perovskite solar cells using the modified solvent engineering technique developed by the authors. To date, most planar perovskite solar cells have employed TiO_2 or ZnO as the ETL, which serves the dual function of a hole blocking and an electron extraction layer. By introducing a double ETL into the N-I-P device using the low-temperature fabricated TiO_2 and PCBM, the role of a single PCBM layer in the device could be clarified. Instead of PEI, a dense and thin TiO_2 layer was first deposited on top of the ITO substrate and the remaining fabrication steps were identical to those employed when a device employing a single PCBM layer is fabricated. The modified solvent engineering process presented herein is considered reproducible and also enabled formation of a double ETL device with the ITO/bl-TiO_2/PCBM/$MAPbI_3$/PTAA/Au configuration, as displayed in Fig. 4a. As shown in Fig. 4b, the PCE (15.2%) of the double ETL device was comparable to that (15.3%) achieved with the device employing a single PCBM layer. The device parameters for the double ETL device are J_{sc} = 20.3 mA cm^{-2}, V_{oc} = 1.03 V, and FF = 72.1%. Hysteresis in J-V curve, similar to that of the single ETL device, was observed; under the forward bias scan, the PCE was 10.0% (see Fig 4b). The resulting device yields a steady-state PCE of 14.0% without any decline in the device performance. (see Fig 4c) Thus, the comparable efficiencies and similar electrical behavior of the single and double ETL devices imply that the single PCBM layer works well as an ETL in the N-I-P configuration, without combination with a metal oxide layer. Finally, as a practical demonstration of a flexible solar cell, we extended this configuration to a flexible ITO/PEN substrate and successfully achieved a PCE of 11.1% (a J_{sc} of 18.7 mA cm^{-2}, a V_{oc} of 0.99 V, and a FF of 60%) in a preliminary test (see Fig. 4d).

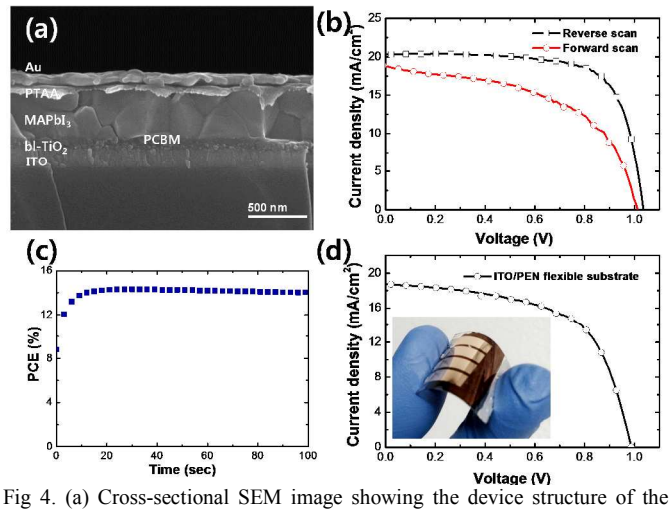

Fig 4. (a) Cross-sectional SEM image showing the device structure of the double ETL-$CH_3NH_3PbI_3$ heterojunction solar cell in the presence of dense-TiO_2 and PCBM. (b) J-V characteristics of double ETL-$CH_3NH_3PbI_3$ heterojunction solar cells, measured under simulated AM 1.5 100 mW cm^{-2} illumination under reverse (black) and forward (red) bias scan, and (c) its steady-state efficiency as a function of time applied at a forward bias of 0.83 V. (d) J-V characteristics of double ETL-$CH_3NH_3PbI_3$ heterojunction solar cells on ITO/PEN substrate, measured under simulated AM 1.5 100 mW cm^{-2} illumination. Inset shows photoimage of the flexible solar cell.

Summary

In summary, metal-oxide-free, efficient perovskite solar cells were fabricated by using the multi-layered FTO/PEI/PCBM/$CH_3NH_3PbI_3$/PTAA/Au configuration. The use of the diethylether drip as an orthogonal solvent in the modified solvent engineering process enabled formation of a dense and uniform thin perovskite layer without damage to the previously deposited PEI and PCBM layers. The optimized device with an approximately 55 nm thick PCBM layer afforded an overall PCE of 15.3% and a steady-state efficiency of 13.9% under standard AM 1.5G 100 mW·cm^{-2} illumination. The use of the low-temperature processed dense-TiO_2 layer in conjunction with the PCBM layer resulted in efficiency comparable to that of the single PCBM device, and enabled fabrication of a flexible solar cell with a PCE of 11.1%. Thus, this study provides a new route for fabricating the N-I-P device architecture via a simple and facile solution process and presents great potential for achieving a large-area, low-temperature, and flexible photovoltaic device. Furthermore, the incorporation of PCBM into the top cell as an ETL should further extend this device architecture into tandem cell application.

Acknowledgements

This research was supported by the Global Research Laboratory (GRL) Program, the Global Frontier R&D Program of the Center for Multiscale Energy System funded by the National Research Foundation in Korea, and by a grant from the KRICT 2020 Program for Future Technology of the Korea Research Institute of Chemical Technology (KRICT), Republic of Korea.

Notes and references

[a] Division of Advanced Materials, Korea Research Institute of Chemical Technology, 141 Gajeong-Ro, Yuseong-Gu, Daejeon 305-600, Repulbic of Korea.
[b] Department of Energy Science, Sungkyunkwan University, Suwon 440-746, Republic of Korea.
[§] These authors contributed equally to this work.
† Electronic Supplementary Information (ESI) available: A description on detailed experimental process, and characterization. See DOI: 10.1039/c000000x/
* To whom correspondence should be addressed. E-mail: seoksi@krict.re.kr (seoksi@skku.edu)

1. K. Liang, D. B. Mitzi and M. T. Prikas, *Chem. Mater.* 1998, **10**, 403-411.
2. A. Kojima, K.Teshima, Y. Shirai and T. Miyasaka, *J. Am. Chem. Soc.* 2009, **131**, 6050-6051.
3. J.-H. Im, C. R. Lee, J. W. Lee, S. W. Park and N. G. Park, *Nanoscale* 2011, **3**, 4088-4093.
4. L. Etgar, P. Gao, Z. S. Xue, Q. Peng, A. K. Chandiran, B. Liu, M. K. Nazeeuddin and M. Graztel, *J. Am. Chem. Soc.* 2012, **134**, 17396-17399.

5. M. M. Lee, J. Teuscher, T. Miyasaka, T. N. Murakami and H. J. Snaith, *Science* 2012, **338**, 643-647.
6. H.-S. Kim, C.-R. Lee, J.-H. Im, K.-B. Lee, T. Moehl, A. Marchioro, S.-J. Moon, R. Humphry-Baker, J.-H. Yum, J. E. Moser, M. Grätzel, and N.-G. Park, *Sci. Rep.* 2012, **2**, 1-7.
7. J. H. Noh, S. H. Im, J. H. Heo, T. N. Mandal and S. I. Seok, *Nano Lett*., 2013, **13**, 1764−1769.
8. J. H. Heo, S. H. Im, J. H. Noh, T. N. Mandal, C.-S. Lim, J. A. Chang, Y. H. Lee, H. Kim, A. Sarkar, M. K. Nazeeruddin, M. Grätzel and S. I. Seok, *Nat. Photon.* 2013, **7**, 486-491.
9. J. Burschka, N. Pellet, S.-J. Moon, R. Humphry-Baker, P. Gao, M. K. Nazeeruddin and M. Grätzel, *Nature*, 2013, **499**, 316-319.
10. M. Liu, M. B. Johnston and H. J. Snaith, *Nature*, 2013, **501**, 395-398.
11. H. J. Snaith, *J. Phys. Chem. Lett.* 2013, **4**, 3623-3630.
12. M. D. McGehee, *Nature* 2013, **501**, 323–325.
13. S. Ryu, J. H. Noh, N. J. Jeon, Y. C. Kim, W. S. Yang, J. Seo, S. I. Seok, *Energy Environ. Sci.* 2014, **7**, 2614-2618.
14. G. C. Xing, N. Mathews, S. Sun, S. S. Lim, Y. M. Lam, M. Grätzel, S. Mhaisalkar and T. C. Sum, *Science*, 2013, **342**, 344-347.
15. S. D. Stranks, G. E. Eperon, G. Grancini, C. Menelaou, M. J. P. Alcocer, T. Leijtens, L. M. Herz, A. Petrozza and H. J. Snaith, *Science*, 2013, **342**, 341-344.
16 N. J. Jeon, H. G. Lee, Y. C. Kim, J. Seo, J. H. Noh, J. Lee, S. I. Seok, *J. Am. Chem. Soc.* 2014, **136**, 7837-7840.
17. G. E. Eperon, S. D. Stranks, C. Menelaou, M. B. Johnston, L. M. Herz and H. J. Snaith, *Energy Environ. Sci.* 2014, **7**, 982-988.
18. N. J. Jeon, J. H. Noh, Y. C. Kim, W. S. Yang, S. Ryu, S. I. Seok, *Nat. Mater.* 2014, **13**, 897-903.
19. N. J. Jeon, J. H. Noh, W. S. Yang, Y. C. Kim, S. Ryu, J. Seo, S. I. Seok, *Nature* (in press).
20. Research Cell Efficiency Records *(*National Renewable Energy Laboratory*)* *http://www.nrel.gov/ncpv/images/efficiency_chart.jpg*..
21. J. M. Ball, M. M. Lee, A. Hey, H. J. Snaith, *Energy Environ. Sci.* 2013, **6**, 1739-1743.
22. J. T. Wang, J. M. Ball, E. M. Barea, A. Abate, J. A. Alexander-Webber, J. Huang, M. Saliba, I. Mora-Sero, J. Bisquert, H. J. Snaith, *Nano Lett*., 2014, **14**, 724−730.
23. D. Liu and T. L. Kelly, *Nat. Photonics* 2014, **8**, 133-138.
24. H. Zhou, Q. Chen, G. Li, S. Luo, T.-B. Song, H.-S. Duan, Z. Hong, J. You, Y. Liu, Y. Yang, *Science* 2014, **345**, 542-546.
25. J. Kim, G. Kim, T. K. Kim, S. Kwon, H. Back, J. Lee, S. H. Lee, H. Kang, K. Lee, *J. Mater. Chem. A*. 2014, **2**, 17291-17296.
26. Z. Wei, H. Chen, K. Yan, S. Yang, *Angew. Chem. Int. Ed.* 2014, **53**, 1-6.
27. A. T. Barrows, A. J. Pearson, C. K. Kwak, A. D. F. Dunbar, A. R. Buckley, D. G. Lidzey, *Energy Environ. Sci.* 2014, **7**, 2944-2950.
28. J. Y. Jeng, Y. F. Chiang, M. H. Lee, S. R. Peng, T. F. Guo, P. Chen and T. C. Wen, *Adv. Mater.* 2013, **25**, 3727-3732.
29. S. Y. Sun, T. Salim, N. Mathews, M. Duchamp, C. Boothroyd, G. Xing, T. C. Sum and Y. M. Lam, *Energy Environ. Sci.* 2014, **7**, 399-407.
30. P. Docampo, J. M. Ball, M. Darwich, G. E. Eperon and H. J. Snaith, *Nat. Commun.* 4:2761 DOI: 10.1038/ncomms*3761*.
31. O. Malinkiewicz, A. Yella, Y. H. Lee, G. M. Espallargas, M. Graetzel, M. K. Nazeeruddin and H. J. Bolink, *Nat. Photonics* 2014, **8**, 133-138.
32. J. You, Z. Hong, Y. M. Yang, Q. Chen, M. Cai, T.-B. Song, C.-C. Chen, S. Lu, Y. Liu, H. Zhou and Y. Yang, *ACS Nano* 2014, **8**, 1674-1680.
33. J. Seo, S. Park, Y. C. Kim, N, J. Nam, J. H. Noh, S. C. Yoon, S. I. Seok, *Energy Environ. Sci.* 2014, **7**, 2642-2646.
34. Q. Wang, Y. Shao, Q. Dong, Z. Xiao, Y. Yuan, J. Huang, *Energy Environ. Sci.* 2014, **7**, 2359-2365.
35. Z. Xiao, Q. Dong, C. Bi, Y. Shao, Y. Yuan, J. Huang, *Adv. Mater.* 2014, **26**, 6503-6509.
36. M. Jorgensen, K. Norrman, F. C. Krebs, Sol. Energy Mater. Sol. Cells 2008, 92, 686-714.
37. Y. Zhou, C. Fuentes-Hernandez, J. Shim, J. Meyer, A. J. Giordano, H. Li, P. Winget, T. Papadopoulos, H. Cheun, J. Kim *et. al*, *Science* 2012, **336**, 327-332.
38. H. Kang, S. Hong, J. Lee, K. Lee, *Adv. Mater.* 2014, **24**, 3005-3009.
39. F. B. Kooistra, V. D. Mihailetchi, L. M. Popescu, D. Kronholm, P.W. M. Blom, J. C. Hummelen, *Chem. Mater.* 2006, **18**, 3068-3073.
40. H. J. Snaith, A. Abate, J. M. Ball, G. E. Eperon, T. Leijtens, N. K. Noel, S. D. Stranks, J. T. Wang, K. Wojciechowski, W. Zhang, *J. Phys. Chem. Lett.* 2014, **5**, 1511-1515.
41. E. L. Unger, E. T. Hoke, C. D. Bailie, W. H. Nguyen, A. R. Bowring, T. Heumuller, M. G. Christoforo, M. D. McGehee, *Energy Environ. Sci.* 2014, **7**, 3690-3698.